EUROPEAN ORGANISATION FOR PARTICLE PHYSICS

CERN-PPE/93-79
12 May, 1993

A Measurement of $\Gamma(Z^0 \to b\bar{b})/\Gamma(Z^0 \to \text{hadrons})$ Using an Impact Parameter Technique

The OPAL Collaboration

Abstract

The fractional partial width of the Z^0 to b quarks, $\Gamma_{b\bar{b}}/\Gamma_{had}$, has been measured by OPAL using an impact parameter technique. The method has been developed using 130 000 hadronic events collected by OPAL in 1990. We find:

$$\frac{\Gamma_{b\bar{b}}}{\Gamma_{had}} = 0.222 \pm 0.007\ (\text{stat}) \pm 0.008\ (\text{sys}).$$

The measurement assumes the relative rates of the Z^0 to uds and c quarks given by the Standard Model. Varying the charm fraction from the Standard Model value of $\Gamma_{c\bar{c}}/\Gamma_{had}$=0.171 changes the result by an additional $\Delta\Gamma_{b\bar{b}}/\Gamma_{b\bar{b}} = -0.135 \times \Delta\Gamma_{c\bar{c}}/\Gamma_{c\bar{c}}$.

(Submitted to Zeitschrift für Physik C)

The OPAL Collaboration

P.D. Acton[25], R. Akers[16], G. Alexander[23], J. Allison[16], K.J. Anderson[9], S. Arcelli[2], A. Astbury[28], D. Axen[29], G. Azuelos[18,a], J.T.M. Baines[16], A.H. Ball[17], J. Banks[16], R.J. Barlow[16], S. Barnett[16], R. Bartoldus[3], J.R. Batley[5], G. Beaudoin[18], A. Beck[23], G.A. Beck[13], J. Becker[10], C. Beeston[16], T. Behnke[27], K.W. Bell[20], G. Bella[23], P. Bentkowski[18], P. Berlich[10], S. Bethke[11], O. Biebel[3], I.J. Bloodworth[1], P. Bock[11], B. Boden[3], H.M. Bosch[11], M. Boutemeur[18], H. Breuker[8], P. Bright-Thomas[25], R.M. Brown[20], A. Buijs[8], H.J. Burckhart[8], C. Burgard[27], P. Capiluppi[2], R.K. Carnegie[6], A.A. Carter[13], J.R. Carter[5], C.Y. Chang[17], D.G. Charlton[8], S.L. Chu[4], P.E.L. Clarke[25], J.C. Clayton[1], I. Cohen[23], J.E. Conboy[15], M. Cooper[22], M. Coupland[14], M. Cuffiani[2], S. Dado[22], G.M. Dallavalle[2], S. De Jong[13], L.A. del Pozo[5], H. Deng[17], A. Dieckmann[11], M. Dittmar[4], M.S. Dixit[7], E. do Couto e Silva[12], J.E. Duboscq[8], E. Duchovni[26], G. Duckeck[11], I.P. Duerdoth[16], D.J.P. Dumas[6], P.A. Elcombe[5], P.G. Estabrooks[6], E. Etzion[23], H.G. Evans[9], F. Fabbri[2], B. Fabbro[21], M. Fierro[2], M. Fincke-Keeler[28], H.M. Fischer[3], D.G. Fong[17], M. Foucher[17], A. Gaidot[21], J.W. Gary[4], J. Gascon[18], N.I. Geddes[20], C. Geich-Gimbel[3], S.W. Gensler[9], F.X. Gentit[21], G. Giacomelli[2], R. Giacomelli[2], V. Gibson[5], W.R. Gibson[13], J.D. Gillies[20], J. Goldberg[22], D.M. Gingrich[30,a], M.J. Goodrick[5], W. Gorn[4], C. Grandi[2], F.C. Grant[5], J. Hagemann[27], G.G. Hanson[12], M. Hansroul[8], C.K. Hargrove[7], P.F. Harrison[13], J. Hart[8], P.M. Hattersley[1], M. Hauschild[8], C.M. Hawkes[8], E. Heflin[4], R.J. Hemingway[6], G. Herten[10], R.D. Heuer[8], J.C. Hill[5], S.J. Hillier[8], T. Hilse[10], D.A. Hinshaw[18], J.D. Hobbs[8], P.R. Hobson[25], D. Hochman[26], R.J. Homer[1], A.K. Honma[28,a], R.E. Hughes-Jones[8], R. Humbert[10], P. Igo-Kemenes[11], H. Ihssen[11], D.C. Imrie[25], A.C. Janissen[6], A. Jawahery[17], P.W. Jeffreys[20], H. Jeremie[18], M. Jimack[1], M. Jones[29], R.W.L. Jones[8], P. Jovanovic[1], C. Jui[4], D. Karlen[6], K. Kawagoe[24], T. Kawamoto[24], R.K. Keeler[28], R.G. Kellogg[17], B.W. Kennedy[15], S. Kluth[5], T. Kobayashi[24], D.S. Koetke[8], T.P. Kokott[3], S. Komamiya[24], L. Köpke[8], J.F. Kral[8], R. Kowalewski[6], J. von Krogh[11], J. Kroll[9], M. Kuwano[24], P. Kyberd[13], G.D. Lafferty[16], H. Lafoux[21], R. Lahmann[17], F. Lamarche[18], J.G. Layter[4], P. Leblanc[18], A.M. Lee[31], M.H. Lehto[15], D. Lellouch[26], C. Leroy[18], J. Letts[4], S. Levegrün[3], L. Levinson[26], S.L. Lloyd[13], F.K. Loebinger[16], J.M. Lorah[17], B. Lorazo[18], M.J. Losty[7], X.C. Lou[12], J. Ludwig[10], A. Luig[10], M. Mannelli[8], S. Marcellini[2], C. Markus[3], A.J. Martin[13], J.P. Martin[18], T. Mashimo[24], P. Mättig[3], U. Maur[3], J. McKenna[28], T.J. McMahon[1], J.R. McNutt[25], F. Meijers[8], D. Menszner[11], F.S. Merritt[9], H. Mes[7], A. Michelini[8], R.P. Middleton[20], G. Mikenberg[26], J. Mildenberger[6], D.J. Miller[15], R. Mir[12], W. Mohr[10], C. Moisan[18], A. Montanari[2], T. Mori[24], M. Morii[24], U. Müller[3], B. Nellen[3], H.H. Nguyen[9], S.W. O'Neale[1], F.G. Oakham[7], F. Odorici[2], H.O. Ogren[12], C.J. Oram[28,a], M.J. Oreglia[9], S. Orito[24], J.P. Pansart[21], B. Panzer-Steindel[8], P. Paschievici[26], G.N. Patrick[20], N. Paz-Jaoshvili[23], M.J. Pearce[1], P. Pfister[10], J.E. Pilcher[9], J. Pinfold[30], D. Pitman[28], D.E. Plane[8], P. Poffenberger[28], B. Poli[2], A. Pouladdej[6], T.W. Pritchard[13], H. Przysiezniak[18], G. Quast[27], M.W. Redmond[8], D.L. Rees[8], G.E. Richards[16], S.A. Robins[13], D. Robinson[8], A. Rollnik[3], J.M. Roney[28,b], E. Ros[8], S. Rossberg[10], A.M. Rossi[2], M. Rosvick[28], P. Routenburg[6], K. Runge[10], O. Runolfsson[8], D.R. Rust[12], M. Sasaki[24], C. Sbarra[2], A.D. Schaile[10], O. Schaile[10],

W. Schappert[6], P. Scharff-Hansen[8], P. Schenk[4], B. Schmitt[3], H. von der Schmitt[11], M. Schröder[12], C. Schwick[27], J. Schwiening[3], W.G. Scott[20], M. Settles[12], T.G. Shears[5], B.C. Shen[4], C.H. Shepherd-Themistocleous[7], P. Sherwood[15], G.P. Siroli[2], A. Skillman[16], A. Skuja[17], A.M. Smith[8], T.J. Smith[28], G.A. Snow[17], R. Sobie[28,b], R.W. Springer[17], M. Sproston[20], A. Stahl[3], C. Stegmann[10], K. Stephens[16], J. Steuerer[28], R. Ströhmer[11], D. Strom[19], H. Takeda[24], T. Takeshita[24,c], S. Tarem[26], M. Tecchio[9], P. Teixeira-Dias[11], N. Tesch[3], M.A. Thomson[15], E. Torrente-Lujan[22], S. Towers[28], G. Transtromer[25], N.J. Tresilian[16], T. Tsukamoto[24], M.F. Turner[8], D. Van den plas[18], R. Van Kooten[27], G.J. VanDalen[4], G. Vasseur[21], C.J. Virtue[7], A. Wagner[27], D.L. Wagner[9], C. Wahl[10], C.P. Ward[5], D.R. Ward[5], P.M. Watkins[1], A.T. Watson[1], N.K. Watson[8], M. Weber[11], P. Weber[6], P.S. Wells[8], N. Wermes[3], M.A. Whalley[1], B. Wilkens[10], G.W. Wilson[4], J.A. Wilson[1], V-H. Winterer[10], T. Wlodek[26], G. Wolf[26], S. Wotton[11], T.R. Wyatt[16], R. Yaari[26], A. Yeaman[13], G. Yekutieli[26], M. Yurko[18], W. Zeuner[8], G.T. Zorn[17].

[1]School of Physics and Space Research, University of Birmingham, Birmingham, B15 2TT, UK
[2]Dipartimento di Fisica dell' Università di Bologna and INFN, Bologna, 40126, Italy
[3]Physikalisches Institut, Universität Bonn, D-5300 Bonn 1, Germany
[4]Department of Physics, University of California, Riverside, CA 92521 USA
[5]Cavendish Laboratory, Cambridge, CB3 0HE, UK
[6]Carleton University, Dept of Physics, Colonel By Drive, Ottawa, Ontario K1S 5B6, Canada
[7]Centre for Research in Particle Physics, Carleton University, Ottawa, Ontario K1S 5B6, Canada
[8]CERN, European Organisation for Particle Physics, 1211 Geneva 23, Switzerland
[9]Enrico Fermi Institute and Dept of Physics, University of Chicago, Chicago Illinois 60637, USA
[10]Fakultät für Physik, Albert Ludwigs Universität, D-7800 Freiburg, Germany
[11]Physikalisches Institut, Universität Heidelberg, Heidelberg, Germany
[12]Indiana University, Dept of Physics, Swain Hall West 117, Bloomington, Indiana 47405, USA
[13]Queen Mary and Westfield College, University of London, London, E1 4NS, UK
[14]Birkbeck College, London, WC1E 7HV, UK
[15]University College London, London, WC1E 6BT, UK
[16]Department of Physics, Schuster Laboratory, The University, Manchester, M13 9PL, UK
[17]Department of Physics, University of Maryland, College Park, Maryland 20742, USA
[18]Laboratoire de Physique Nucléaire, Université de Montréal, Montréal, Quebec, H3C 3J7, Canada
[19]University of Oregon, Dept of Physics, Eugene, Oregon 97403, USA
[20]Rutherford Appleton Laboratory, Chilton, Didcot, Oxfordshire, OX11 0QX, UK
[21]DAPNIA/SPP, Saclay, F-91191 Gif-sur-Yvette, France
[22]Department of Physics, Technion-Israel Institute of Technology, Haifa 32000, Israel
[23]Department of Physics and Astronomy, Tel Aviv University, Tel Aviv 69978, Israel
[24]International Centre for Elementary Particle Physics and Dept of Physics, University of

Tokyo, Tokyo 113, and Kobe University, Kobe 657, Japan
[25]Brunel University, Uxbridge, Middlesex, UB8 3PH UK
[26]Nuclear Physics Department, Weizmann Institute of Science, Rehovot, 76100, Israel
[27]Universität Hamburg/DESY, II Inst für Experimental Physik, 2000 Hamburg 52, Germany
[28]University of Victoria, Dept of Physics, P O Box 3055, Victoria BC V8W 3P6, Canada
[29]University of British Columbia, Dept of Physics, Vancouver BC V6T 1Z1, Canada
[30]University of Alberta, Dept of Physics, Edmonton AB T6G 2N5, Canada
[31]Duke University, Dept of Physics, Durham, North Carolina 27708-0305, USA

[a]Also at TRIUMF, Vancouver, Canada V6T 2A3
[b]And IPP, University of Victoria, Dept of Physics, P O Box 3055, Victoria BC V8W 3P6, Canada
[c]Also at Shinshu University, Matsumoto 390, Japan

1 Introduction

The success of LEP has provided a considerable body of experimental evidence confirming the predictions of the Standard Model of electroweak physics. The partial widths of the Z^0 into hadrons and leptons have been measured to a precision of 1% [1, 2]. The Standard Model prediction for the hadronic width, Γ_{had}, depends on the unknown mass of the top quark. In contrast, cancellations between the contributions of top quark loops to the boson self-energies and $Z^0 \to b\overline{b}$ vertex corrections make the partial width of the Z^0 to b quarks, $\Gamma_{b\overline{b}}$, relatively insensitive to the top quark mass [3]. A precise measurement of $\Gamma_{b\overline{b}}$ will therefore provide a stringent test of the cancellations in the radiative corrections predicted by the Standard Model and restrict the contributions of possible extensions [4].

Previously published measurements of $\Gamma_{b\overline{b}}$ have used leptons produced in the semi-leptonic decay of B hadrons to identify $b\overline{b}$ decays of the Z^0 [5, 6], or have used event shapes, for example, the boosted sphericity product [7]. Combinations of various identification criteria have been used as inputs to artificial neural networks [8]. The Mark II collaboration has used the long lifetime of the B hadron to separate $b\overline{b}$ events from the other quark species produced at the Z^0 peak [9]. In this article we will describe a measurement using a similar lifetime based technique to determine the fractional partial width of the Z^0 to b quarks, $f_{b\overline{b}} = \Gamma_{b\overline{b}}/\Gamma_{\mathrm{had}}$. The present analysis is based on a data sample of 130 000 multihadronic decays of the Z^0 collected by OPAL during the 1990 LEP run, corresponding to an integrated luminosity of $6.6\,\mathrm{pb}^{-1}$. Future applications of this method within OPAL will benefit from both the increasing data samples and the introduction of a silicon micro-vertex detector in 1991.

The $b\overline{b}$ quark-antiquark pairs from a Z^0 decay are produced predominantly back-to-back, and the b and $\overline{b}$ both fragment to B hadrons. These B hadrons carry a substantial fraction of the centre-of-mass energy. Because of the long B hadron lifetime, the trajectories of particles produced in the B hadron decays do not point back to the production point. In contrast, most of the particles produced in light quark events, ($u\overline{u}$, $d\overline{d}$, $s\overline{s}$, and $c\overline{c}$), originate there. Tracks from the decay of a B hadron will intersect the B direction of travel in front of the production point rather than behind it (the B direction is taken to be forward). Tracks from primary particles that do not point back to the production point because of multiple scattering or reconstruction errors will be equally likely to intersect the B direction in front of and behind it. The thrust axis is used to approximate the B hadron direction. Thus $b\overline{b}$ decays of the Z^0 can be selected by requiring the events contain several tracks that intersect the thrust axis in front of the primary vertex (forward tracks). Such a method offers substantially better efficiency than methods using leptons and is insensitive to uncertainties in the branching ratio of B hadrons to leptons, $Br(\mathrm{B} \to \ell\mathrm{X})$. On the other hand, the detector performance and the production and decay of B hadrons must be well understood if the tagging efficiency and background contamination are to be determined accurately.

In principle, the fractional width could be determined by a simple fit to the data if the dis-

tribution of the number of tracks that significantly miss the primary vertex could be calculated reliably via Monte Carlo simulation for both the $b\overline{b}$ and light quark components. However, given the current knowledge of B production and decay, and the difficulty of accurately modelling the detector response, such a result would suffer from large systematic uncertainties associated with the modelling both of B physics and of the detector. The back-to-back nature of the $b\overline{b}$ quark-antiquark pair can be exploited by using the forward track multiplicities in each hemisphere separately. This double-tag technique reduces the sensitivity of $f_{b\overline{b}}$ to the details of B hadron production and decay physics. By selecting events in which one hemisphere preferentially contains a B, the experimental shape of the b forward multiplicity distribution on the other side can be determined. By considering the number of forward and backward tracks (tracks that intersect the B direction behind the production point) separately, the sensitivity of the measurement to modelling of the detector can also be reduced.

The paper begins with a brief description of the OPAL detector, the criteria used to select a sample of multihadron events, and the determination of the primary vertex. The number of tracks in each hemisphere that intersect the thrust axis in front of and behind the primary vertex are defined as the forward and backward multiplicities respectively. A Monte Carlo simulation is used to calculate the distributions of forward and backward multiplicity in hemispheres of $Z^0 \to b\overline{b}$ and other $Z^0 \to$ hadrons events. In addition to the fractional width, two variable parameters relating small changes in the component multiplicity distributions to small changes in the modelling of the B hadron production and decay and detector response, respectively, are fit for. The fractional partial width, $f_{b\overline{b}}$, is determined by fitting the forward multiplicity distribution of the data to the sum of components predicted by the Monte Carlo, while allowing the fit to determine the best value for all three parameters. Finally, the sensitivity of the result to sources of systematic uncertainty such as detector resolution, the B hadron lifetime and B decay multiplicity are discussed.

2 The OPAL Detector and Simulation

OPAL [10] is a general purpose 4π particle detector at one of four interaction regions of the LEP e^+e^- storage ring at CERN. The position and momentum of charged particles produced in the e^+e^- collisions are measured by a system of drift chambers inside a 0.43 T solenoidal magnet. The system consists of three chambers: a precision vertex chamber measuring the position of charged tracks close to the beam; a large cylindrical main drift chamber measuring curvature and angle; and thin drift chambers measuring the z coordinate of charged tracks as they exit the magnetic volume. Outside the solenoid, the energy of particles is measured by a 25 radiation length lead-glass electromagnetic calorimeter and a 5 interaction length iron-streamer tube hadronic calorimeter. Muons are identified by drift chambers and limited streamer tubes surrounding the calorimeters. The luminosity of the beams is monitored by a system of chambers and calorimeters sensitive to electrons and positrons scattered through small angles. The

detector has been described in detail elsewhere [10], but because they are important in this analysis, a brief description of the vertex chamber and the main tracking chamber will be given here.

The vertex chamber is a cylindrical jet-cell drift chamber separated from the interaction region by an 8 cm radius, 1.4 mm thick carbon fibre beam pipe. The chamber is divided into 36 axial sectors of 12 sense wires each, spaced radially between 10.3 and 16.2 cm. Each wire can measure the azimuthal position of a track to an average precision of 50 μm. The main tracking chamber is a jet-cell drift chamber with an outer radius of 1.85 m and a length of 4 m. The chamber is divided into 24 azimuthal sectors of 159 sense wires each, spaced radially between 25 and 184 cm. Each wire can measure the azimuthal position of the track to an average precision of 135 μm. The impact parameter resolution of the two chambers combined for $|\cos\theta| \leq 0.7$ can be approximated as:

$$\sigma^2_{d_{xy}} = \left(\left(\frac{213}{(p_{xy}\sqrt{\sin\theta})^{0.7}} \right)^2 + 35^2 \right) (\mu\mathrm{m})^2 \qquad (1)$$

where p_{xy} is the component of momentum in the x-y plane measured in GeV/c, θ is the polar angle of the track with respect to the z axis[1] and the impact parameter of a charged track is defined as the distance of closest approach in the x-y plane to the primary vertex.

The response of the detector to multihadronic decays of the Z^0 was simulated using a Monte Carlo program. Events produced by the JETSET [11] event generator were passed through a simulation [12] of the detector, and through the entire chain of analysis programs used to reconstruct the data. The events were generated using Lund symmetric fragmentation with parameters that reproduce the measured properties of multihadronic events at the Z^0 peak [13]. B hadrons produced in the fragmentation of b quarks were allowed to decay with a lifetime of $c\tau_B$=0.039 cm. The simulation includes the effects of multiple scattering, secondary interactions, chamber resolution, chamber inefficiencies, and reconstruction inefficiencies.

Several corrections were made to the Monte Carlo to bring it into agreement with the data. For tracks both with and without vertex chamber hits, Gaussian noise was added to the impact parameters of the Monte Carlo tracks to bring the width of the impact parameter distributions as a function of $p_{\mathrm{scat}}=p_{xy}\sqrt{\sin\theta}$ into agreement with the data[2]. The estimated errors for the track impact parameters of both the Monte Carlo and the data were scaled to reproduce the measured resolution of the data. To reproduce the non-Gaussian resolution tail of the data, randomly selected tracks were given large impact parameters according to the non-Gaussian distribution predicted by the Monte Carlo. The relative population of tracks with and without vertex chamber hits was reproduced by degrading the resolution of a small fraction of tracks at

[1] OPAL uses a right-handed coordinate system. Positive z is along the e^- beam direction; ϕ is the azimuthal angle; and θ is the polar angle.

[2] If the resolution was due entirely to a single cylindrical scatterer at a fixed radius from the beam, the r.m.s. impact parameter would be expected to behave as $1/p_{\mathrm{scat}}$.

random. The process was iterated until the Monte Carlo reproduced the width of the resolution peak, the resolution non-Gaussian tail, and the relative track populations to 2 percent or better. The resolution for Monte Carlo tracks with vertex chamber hits was degraded in this way by 18% at 1 GeV.

3 Event and Track Selection

An initial sample of 132 726 multihadronic events was selected from the data collected in 1990 by imposing the same requirements used by OPAL to measure the hadronic width of the Z^0 [14]. The selection required that the vertex chamber, the main tracking chamber, and the electromagnetic calorimeter be in good working order.

Events were used in this analysis only if the measured thrust axis (calculated using charged tracks and calorimeter clusters) was within the range $|\cos\theta_T| \leq 0.866$. This requirement rejects 14% of the events, but ensures that most of the tracks in the event will be detected by the chamber system and eliminates events where the impact parameter of the tracks is more sensitive to the resolution of the detector than to the lifetime of long-lived particles. To suppress events where the quark-antiquark pair was not produced in a back-to-back topology, the thrust of the event was required to be greater than 0.90. The restriction on the thrust rejects a further 23% of the events. The combined event selection requirements reduced the data sample by a factor of 0.632 to 83 837 multihadrons.

The same selection requirements were applied to a sample of 289 947 Monte Carlo events. Of these, 185 374 (63.9%) survived. Of 62 893 $Z^0 \to b\overline{b}$ Monte Carlo events in the generated sample, 40 121 (63.8%) met the selection criteria. Thus there is no evidence the event selection introduces any bias in the $b\overline{b}$ fraction of the data sample.

Charged tracks in the events were used in the analysis only if they had:

- a transverse momentum with respect to the beam axis of more than 0.1 GeV/c;
- a momentum greater than 0.15 GeV/c;
- an impact parameter with respect to the beam spot of less than 2.0 cm;
- more than 50 space points (of a possible 159) measured by the main tracking chamber; and
- they missed the beam spot by less than 20 cm in z.

The efficiency of each of these cuts individually was reproduced by the Monte Carlo to better than 2%, while the number of Monte Carlo tracks per event surviving the combination of all six requirements agreed with the data to within 0.1%.

4 Primary Vertex Determination

An initial determination of the primary vertex position for each event was made by fitting the selected tracks to a common vertex, rejecting the track with the largest contribution to χ^2 for the fit, and repeating this process until all tracks were within 3 standard deviations of the common vertex. This determination was combined with the position of the beam centroid [15] using a weighted average, taking into account the width of the beam spot and the uncertainty in its position, to obtain the final beam-constrained primary vertex position.

The x and y distributions of the unconstrained primary vertex with respect to the beam centroid are shown in Figures 1(a) and 1(b). The data is well modelled by the Monte Carlo. The effective y spot size, σ_y=27 μm, is dominated by the uncertainty in the beam position, while the effective x spot size σ_x=157 μm, is dominated by the physical width of the beam. The separation, $(X_{\mathrm{primary}} - X_{\mathrm{IP}})/\sigma$ of the unconstrained primary vertex from the beam centroid is shown in Figures 1(c) and 1(d). The width of the data distribution is reproduced by the Monte Carlo to within 1%.

5 The Forward and Backward Multiplicity

The signed impact parameter for a charged track was defined as illustrated in Figure 2:

$$d_{\mathrm{sign}} = \mathrm{Sign}((d_{xy} \cdot T_{xy})(p_{xy} \cdot T_{xy}))|d_{xy}|; \qquad (2)$$

where d_{xy} is the vector in the x-y plane from the primary vertex to the point of closest approach of the track; T_{xy} is the component of the thrust axis in the same plane; and p_{xy} is the x-y momentum of the track. With this sign convention, tracks produced by the decay of a long-lived particle travelling along the thrust axis will be preferentially assigned a positive impact parameter. Due to the detector resolution, the tracks of particles that originate at the primary vertex will be assigned positive and negative impact parameters with equal probability.

Figure 3 shows the signed impact parameter distribution for all tracks that satisfy the selection criteria, while Figure 4 shows the distribution of the signed separation, $d_{\mathrm{sign}}/\sigma_d$. The dashed curves on the two plots show the distributions for Monte Carlo events where the Z^0 decayed via the $b\overline{b}$ channel. Both the peak and the tails of the data distributions are in reasonable agreement with the Monte Carlo. There is an excess of data tracks with intermediate

values ($\pm 5\sigma$) of signed separation because the Monte Carlo does not adequately describe the impact parameters of low momentum tracks with no vertex chamber hits.

It is apparent from Figures 3 and 4 that many of the tracks with positive signed impact parameter come from $b\bar{b}$ decays of the Z^0. Up to 40% of the tracks with a separation of more than 2.6σ come from $b\bar{b}$ decays of the Z^0, while there is little enhancement of the $b\bar{b}$ signal for impact parameters beyond 0.3 cm. A track was classified as a forward track if it had a positive separation greater than 2.6σ and a signed impact parameter less than 0.3 cm:

- Forward Track: $2.6 \leq d_{\rm sign}/\sigma_d$ and $d_{\rm sign} \leq 0.3\,{\rm cm}$.

Similarly, backward tracks were defined to be those tracks with signed separation less than -2.6σ and an impact parameter greater than -0.3 cm:

- Backward Track: $d_{\rm sign}/\sigma_d \leq -2.6$ and $-0.3\,{\rm cm} \leq d_{\rm sign}$.

By requiring several forward tracks, $b\bar{b}$ decays of the Z^0 can be selected with high purity and good efficiency. Figure 5 shows the distribution of signed separation for all tracks, forward tracks, and backward tracks. The low momentum tracks without vertex hits that produce the excess at $\pm 5\sigma$ in the distribution of all tracks are rejected by the requirement that the magnitude of the impact parameter be less than 0.3 cm.

The number of forward (backward) tracks in each event was defined as the forward (backward) multiplicity of that event. The forward and backward multiplicity distributions for the Monte Carlo sample are shown in Figures 6 and 7 respectively.

The shape of the multiplicity distributions for light quark (udsc) events is determined by the resolution of the detector. Both the forward and backward tracks in these events are predominantly tracks from the primary vertex reconstructed with a large impact parameter due to detector resolution. The forward and backward multiplicity distributions for these events are similar in shape. Although the average decay length of weakly decaying charmed particles at LEP is similar to that of the B hadrons, the forward multiplicity distribution of the $c\bar{c}$ events is closer to that of the uds events than that of the $b\bar{b}$ events due to the lower mean decay multiplicity of the charmed hadrons.

The backward multiplicity distribution for $b\bar{b}$ events is similar to the distributions for the light quarks. In contrast, the forward distribution for $b\bar{b}$ events has a distinctly different shape. Because the tracks from B decays are preferentially given a positive sign, the $b\bar{b}$ events have a higher mean forward multiplicity than light quark events.

The difference in shape of the forward multiplicity distributions for $b\bar{b}$ events and the other quark species produced at the Z^0 allows these events to be separated from each other on a statistical basis.

6 Fitting the Fractional Width

If the Monte Carlo could accurately predict the shapes of the forward multiplicity distributions for both light quark decays, $P_{\mathrm{udsc}}(n)$, and $\mathrm{b\bar{b}}$ decays, $P_{\mathrm{b\bar{b}}}(n)$, of the Z^0, the fractional width, $f_{\mathrm{b\bar{b}}}$, could be determined by binning the data events according to their forward multiplicity, n, and fitting the distribution to the form:

$$P(n) = (1 - f_{\mathrm{b\bar{b}}})P_{\mathrm{udsc}}(n) + f_{\mathrm{b\bar{b}}}P_{\mathrm{b\bar{b}}}(n). \tag{3}$$

It is possible to modify the fit to take into account discrepancies between the Monte Carlo predictions and the true forward multiplicity distributions of the data.

The thrust axis was used to divide the event into two hemispheres, and each of the tracks in an event was assigned to one of the two. The data was binned in n_1, and n_2, the forward multiplicity in the respective hemispheres:

$$\begin{aligned} n &\rightarrow n_1 + n_2 \\ P(n) &\rightarrow P(n_1, n_2) \\ P_{\mathrm{udsc}}(n) &\rightarrow P_{\mathrm{udsc}}(n_1, n_2) \\ P_{\mathrm{b\bar{b}}}(n) &\rightarrow P_{\mathrm{b\bar{b}}}(n_1, n_2). \end{aligned} \tag{4}$$

The back-to-back nature of the $\mathrm{b\bar{b}}$ pairs produced at the Z^0 allows the fit to effectively select $\mathrm{b\bar{b}}$ events using one hemisphere, and determine the shape of the b forward multiplicity distribution from the opposite hemisphere. The backward multiplicity of the data can be used to correct the Monte Carlo distributions for the resolution of the detector, and hence determine the forward multiplicity distribution for udsc events, $P_{\mathrm{udsc}}(n_1, n_2)$.

For example, if the average B hadron lifetime is underestimated in the Monte Carlo, the simulation will underestimate the forward multiplicity of the data. Whereas a B decay with a decay length comparable to the resolution of the detector might produce two forward tracks, an otherwise identical decay generated with a slightly longer average B hadron lifetime might produce three forward tracks. The net result of a small increase in the average B hadron lifetime will be that some fraction of the hemispheres containing a B decay will have an additional forward track.

If a fraction, x, of b hemispheres contain an additional forward track[3], the true forward multiplicity distribution for a hemisphere containing a b decay will be

$$P_{\mathrm{b}}(n_1|x) = (1 - x)P_{\mathrm{b}}(n_1) + xP_{\mathrm{b}}(n_1 - 1). \tag{5}$$

[3]Alternatively, x can be thought of as the increase in the mean number of forward tracks in the hemisphere: $\overline{n} = (1 - x)\overline{n}_{\mathrm{MC}} + x(\overline{n}_{\mathrm{MC}} + 1)$ implying that $\overline{n} = \overline{n}_{\mathrm{MC}} + x$.

If the correction to one hemisphere is assumed to be independent of the distribution in the other, the joint distribution for the forward multiplicities, n_1 and n_2, in the two hemispheres will be:

$$\begin{aligned} P_{b\bar{b}}(n_1,n_2|x) &= (1-x)^2 P_{b\bar{b}}(n_1,n_2) \\ &\quad +x(1-x)(P_{b\bar{b}}(n_1-1,n_2)+P_{b\bar{b}}(n_1,n_2-1)) \\ &\quad +x^2 P_{b\bar{b}}(n_1-1,n_2-1). \end{aligned} \tag{6}$$

The fractional width, $f_{b\bar{b}} = \Gamma_{b\bar{b}}/\Gamma_{had}$, can then be determined by fitting the forward multiplicity distribution of the data to the form

$$P(n_1,n_2|f_{b\bar{b}},x) = (1-f_{b\bar{b}})P_{udsc}(n_1,n_2) + f_{b\bar{b}}P_{b\bar{b}}(n_1,n_2|x), \tag{7}$$

to find the optimum value of $f_{b\bar{b}}$, while treating x as a free parameter. To first order, the Monte Carlo will account for geometric and kinematic correlations. The additional parameter, x, will allow the fit to make small changes to the shape of the $b\bar{b}$ multiplicity distribution predicted by the Monte Carlo so as to get the best agreement with the distribution of the data in one hemisphere when the forward multiplicity in the other indicates the events are likely to be $b\bar{b}$ decays.

To take into account uncertainties in the peak width and non-Gaussian tails of the resolution used to generate the Monte Carlo events, an additional degree of freedom was allowed in the fit. The resolution of the detector determines the shapes of both the forward and backward multiplicity distributions, and the backward multiplicity of the data can be used to correct the forward multiplicity predicted by the Monte Carlo. In exactly the same fashion as the $b\bar{b}$ distribution was modified to take into account the possibility of additional forward tracks, the Monte Carlo forward and backward multiplicity distributions for both udsc and $b\bar{b}$ events were modified to take into account the possibility that small changes in the Monte Carlo resolution could add an additional forward or backward track to some fraction, t, of both the udsc and $b\bar{b}$ hemispheres:

$$\begin{aligned} P^{for}_{udsc}(n_1,n_2) &\rightarrow P^{for}_{udsc}(n_1,n_2|t); \\ P^{for}_{b\bar{b}}(n_1,n_2|x) &\rightarrow P^{for}_{b\bar{b}}(n_1,n_2|x,t); \\ P^{back}_{udsc}(n_1,n_2) &\rightarrow P^{back}_{udsc}(n_1,n_2|t); \text{ and} \\ P^{back}_{b\bar{b}}(n_1,n_2) &\rightarrow P^{back}_{b\bar{b}}(n_1,n_2|t). \end{aligned} \tag{8}$$

The parameter, t, will allow the fit to simultaneously change the shapes of the Monte Carlo forward and backward distributions. The value of t will be determined primarily by the backward multiplicity distribution of the data. Because the shapes of the backward distributions for both udsc and $b\bar{b}$ events and the forward distribution for udsc events are determined primarily by the resolution of the detector, this effectively allows the fit to determine the shape of the udsc forward distribution from the data. Asymmetries between the backward and forward distributions due to strange and charm particle production are taken into account in the Monte Carlo

distributions. Because the shape of the $b\bar{b}$ backward multiplicity distribution, $P^{\rm back}_{b\bar{b}}(n_1,n_2|t)$, is primarily determined by the resolution of the detector, it is expected to depend only on the parameter t.

Thus the data was fit to the functional forms:

$$\begin{aligned} P^{\rm for}(n_1,n_2|f_{b\bar{b}},x,t) &= (1-f_{b\bar{b}})P^{\rm for}_{\rm udsc}(n_1,n_2|t) + f_{b\bar{b}}P^{\rm for}_{b\bar{b}}(n_1,n_2|x,t); \text{ and} \\ P^{\rm back}(n_1,n_2|f_{b\bar{b}},t) &= (1-f_{b\bar{b}})P^{\rm back}_{\rm udsc}(n_1,n_2|t) + f_{b\bar{b}}P^{\rm back}_{b\bar{b}}(n_1,n_2|t); \end{aligned} \tag{9}$$

to find the best values of $f_{b\bar{b}}$, x, and t.

Tables 1 and 2 give the distributions of forward and backward multiplicity respectively for the data, udsc, and $b\bar{b}$ Monte Carlo events. The Monte Carlo distributions were calculated by binning the udsc and $b\bar{b}$ Monte Carlo events separately in the same way. The $b\bar{b}$ events were weighted to reproduce the average B lifetime of $c\tau_{\rm B}$=0.041±0.003 cm previously measured by OPAL [16]. The distributions were symmetrized in n_1 and n_2, and a combined χ^2 was defined as follows:

$$\begin{aligned} \chi^2(f_{b\bar{b}},x,t) = &\sum_{n_1\geq n_2}\left(\frac{P^{\rm for}_{\rm data}(n_1,n_2) - P^{\rm for}(n_1,n_2|f_{b\bar{b}},x,t)}{\sigma^{\rm for}(n_1,n_2)}\right)^2 + \\ &\sum_{n_1\geq n_2}\left(\frac{P^{\rm back}_{\rm data}(n_1,n_2) - P^{\rm back}(n_1,n_2|f_{b\bar{b}},t)}{\sigma^{\rm back}(n_1,n_2)}\right)^2; \end{aligned} \tag{10}$$

where $\sigma^{\rm for}(n_1,n_2)$ and $\sigma^{\rm back}(n_1,n_2)$ represent the combined statistical error of the data and the Monte Carlo samples for each bin. To ensure that each bin contained enough events that the errors would be normally distributed, the fit was restricted to the bins shown in bold-faced type in Tables 1 and 2.

7 Fit Results

Minimizing χ^2 with respect to $f_{b\bar{b}}$, x, and t yields values of:

$$\begin{aligned} f_{b\bar{b}} &= 0.222 \pm 0.007; \\ x &= 0.102 \pm 0.019; \\ t &= -0.006 \pm 0.002; \\ \rho_{fx} &= -0.894; \\ \rho_{xt} &= +0.233; \\ \rho_{ft} &= -0.442; \\ \chi^2/N_{\rm dof} &= (24.3+12.4)/(19+11-3); \end{aligned}$$

for the parameters and their correlations, ρ. The errors of the fit include Monte Carlo statistics. The $\chi^2/N_{\rm dof}$ of the fit suggests that the functional form chosen for the fit provides an adequate model of the data. The two terms in the numerator represent the individual contributions to $\chi^2/N_{\rm dof}$ of the forward and backward distributions respectively. In Figure 8 the forward multiplicity distribution for the data is compared to the distribution predicted by the Monte Carlo corrected using the results of the fit. The distribution for the Monte Carlo $\rm b\overline{b}$ component is also indicated.

The fractional width is strongly correlated with x. If x is fixed to zero, the $\chi^2/N_{\rm dof}$ is substantially larger, $(54.1 + 13.8)/(19 + 11 - 2)$, and the value of $f_{\rm b\overline{b}}$ determined from the fit is 0.258. The Monte Carlo $\rm b\overline{b}$ events have a mean of 1.0 forward tracks per hemisphere: the value of x from the fit indicates the Monte Carlo underestimates the number of forward tracks in $\rm b\overline{b}$ events by about 10%. Since the mean number of backward tracks per hemisphere is 0.3, the value of t is consistent with a mismatch of 2% between the non-Gaussian resolution tail of the data and the Monte Carlo. The value of x and the large increase in $\chi^2/N_{\rm dof}$ when x is fixed to zero indicate that some aspect of b fragmentation or hadronization or some aspect of B decays is not properly modelled by the Monte Carlo.

The average energy of the B hadrons produced at LEP has been determined using leptons [5, 6], and the average B lifetime has been measured by OPAL to be $c\tau_{\rm B}$=0.041$\pm$0.003 cm [16]. The average multiplicity of $\rm B^0$ and $\rm B^{\pm}$ mesons has been measured at CLEO [17], but the decay multiplicity of the mix of B hadrons produced at LEP is not well known. As will be shown in the next section, the fit is able to compensate for modelling uncertainties in all of these aspects of $\rm Z^0 \to b\overline{b}$ decay, but the values of the parameters determined by the fit can not, by themselves, indicate which particular aspect is improperly modelled.

8 Systematic Uncertainties

The shapes of the multiplicity distributions for the different quark components are determined using the Monte Carlo simulation, and any systematic effect that can cause the shape of these distributions to change can potentially affect the value of $f_{\rm b\overline{b}}$ determined by the fit. The results of systematically varying detector resolution and non-Gaussian tails, beam spot size, B hadron lifetime, decay multiplicity, fragmentation, charm production, the event and track selection criteria and the event generation, are described below. The parameters, $f_{\rm b\overline{b}}$, x, and t were allowed to vary freely as the Monte Carlo parameters and event selection criteria were changed. With the exception of the B hadron lifetime and the B decay multiplicity, x does not show a strong systematic dependence on any of the parameters being varied. The resolution correction, t, is only sensitive to changes in the resolution and the B hadron decay multiplicity.

8.1 Detector Resolution

The Monte Carlo reproduces the impact parameter resolution of the data to better than 2% after the iterative correction procedure described earlier. The systematic uncertainty due to uncertainties in the simulation of detector resolution was estimated by varying the Gaussian noise added to Monte Carlo impact parameter resolution about the optimal value and determining the resulting changes in the fitted partial width. As illustrated in Figure 9, $f_{b\bar{b}}$ is relatively insensitive to the Monte Carlo resolution if t is determined by the fit. If t is fixed to zero, however, $f_{b\bar{b}}$ is far more sensitive to the resolution. The information about the resolution contained in the backward multiplicity distribution allows the fit to reduce the sensitivity of the fractional width to the resolution by a factor of more than two at the cost of a slight increase in the statistical error. Because the resolution is known to better than 2%, the overall systematic uncertainty in the width due to uncertainties in the resolution is: $\Delta f_{b\bar{b}}=\pm 0.001$. Uncertainties in the scaling of the impact parameter errors lead to a negligible uncertainty in the width.

8.2 Non-Gaussian Resolution Tails

The same technique was used to estimate the effect of systematic uncertainties in the non-Gaussian tail of the resolution function. The fraction of tracks in the Monte Carlo tail was varied over a range of $\pm 2\%$. Using the modified Monte Carlo samples in the fit changed $f_{b\bar{b}}$ by 0.001 if t was allowed to vary. In contrast, if t was fixed to zero, the same variation of the Monte Carlo tail fraction resulted in a change of ± 0.011. A systematic uncertainty in the fractional width of $\Delta f_{b\bar{b}}=\pm 0.001$ was attributed to uncertainties in the non-Gaussian tail of the resolution function.

8.3 Beam Spot Size

Varying the horizontal (x) width of the Monte Carlo beam spot by $\pm 5\%$ resulted in a change of the fractional width of less than $\Delta f_{b\bar{b}}=0.001$. Because the corrected Monte Carlo reproduces the beam spot width to 2%, uncertainties associated with the beam spot size were neglected. Systematic uncertainties in the position of the beam centroid are small compared to the width of the beam spot and the impact parameter resolution of the detector and this source of uncertainty was also neglected.

8.4 Average B Hadron Lifetime

The average B hadron lifetime measured by OPAL is $c\tau_B$=0.041$\pm$0.003 cm. The error represents the sum in quadrature of a statistical uncertainty of 0.002 cm and a systematic uncertainty of 0.002 cm. Monte Carlo events were weighted to model average B lifetimes between $c\tau_B$=0.037 cm and 0.045 cm rather than the lifetime of $c\tau_B$=0.039 cm used to generate the events. The weighted samples were then used in the fit. The results are illustrated in Figure 10. If x is fixed to zero, increasing the Monte Carlo lifetime by 10% decreases the fitted width by $\Delta f_{b\bar{b}}$=0.017. When x is determined by the fit, the same percentage change in the lifetime changes $f_{b\bar{b}}$ by less than $\Delta f_{b\bar{b}}$=0.001. Because the B lifetime is known to 7%, a systematic uncertainty in the width of $\Delta f_{b\bar{b}}$=$\pm$0.001 was ascribed to the uncertainty in the lifetime.

8.5 B Hadron Decay Multiplicity

The mean charged decay multiplicity of B^0 and $B^\pm$ mesons has been measured to be 5.50 $\pm$0.03 $\pm$0.15 at CLEO [17]. At LEP, 80% of B hadrons are expected to be B^0 and $B^\pm$ mesons; 12% are expected to be strange B mesons; and 8% are expected to be B baryons. Assuming the decay multiplicity of B hadrons not produced at the Υ(4S) is within one full unit of that of the B^0 and $B^\pm$, the mean charged decay multiplicity of the mix of B hadrons produced at LEP is known to within half a unit. Weighting the Monte Carlo events to vary the mean charged decay multiplicity of B hadrons by $\pm$0.5 changes the width by $\Delta f_{b\bar{b}}$=$\pm$0.004. If x is fixed to zero, the same change in the mean decay multiplicity changes $f_{b\bar{b}}$ by $\Delta f_{b\bar{b}}$=$\pm$0.013.

8.6 b Fragmentation

The uncertainty associated with the modelling of b fragmentation in the Monte Carlo was studied using 980 000 JETSET events produced using an approximate simulation of the detector. The $Z^0 \to b\bar{b}$ events of the sample were weighted to model Peterson [18] fragmentation with values of $\langle x_E \rangle_b$ (the mean fraction of the beam energy carried by the heavy hadron) between 0.68 and 0.73 [5], rather than the Lund symmetric fragmentation used to generate them. Each of the weighted samples in turn were used to analyze the unweighted sample. Because the impact parameters of the tracks from B hadron decays are insensitive to the boost of the B hadron, the fractional width depends only weakly on $\langle x_E \rangle_b$. The fractional width changed by less than $\Delta f_{b\bar{b}}$=$\pm$0.001 as $\langle x_E \rangle_b$ was varied over the range above.

8.7 Charm Production

The charm meson lifetimes are well measured [19], but the relative production rates are not accurately known. JETSET predicts rates for $D^{\pm}$, D^0, $D_s^{\pm}$, and $\Lambda_c^{\pm}$ of 25:54:12:8. Varying the vector to scalar production rates between 2.5:1 and 4:1, and varying the $D_s^{\pm}$ and $\Lambda_c^{\pm}$ fractions between 10–20% and 5–15% respectively varies the $D^{\pm}$ fraction between 20 and 28%. Weighting the Monte Carlo events to vary the $D^{\pm}$ fraction over this range systematically changes $f_{b\bar{b}}$ by $\Delta f_{b\bar{b}}=\pm 0.002$.

In contrast, varying the relative production rates of charm via cascade from B hadrons, will lead to changes in the width similar to the changes caused by varying the average B lifetime. This is accounted for by the x parameter of the fit and leads to a negligible change in the width.

8.8 Charm Fragmentation

The uncertainty in $f_{b\bar{b}}$ associated with the modelling of charm fragmentation was studied by weighting the $Z^0 \to c\bar{c}$ events to model $\langle x_E \rangle_c$ between 0.49 and 0.53 [5]. This changed $f_{b\bar{b}}$ by $\Delta f_{b\bar{b}}=\pm 0.001$. A systematic error of this size was attributed to uncertainties in the modelling of charm fragmentation.

8.9 Charm Partial Width

The Monte Carlo simulation used the Standard Model prediction for the fractional partial width of the Z^0 to charm, $\Gamma_{c\bar{c}}/\Gamma_{had} = 0.171$. The sensitivity of $f_{b\bar{b}}$ to the value of $\Gamma_{c\bar{c}}$ has been investigated by weighting the Monte Carlo $Z^0 \to c\bar{c}$ events to model charm fractions between 0.130 and 0.210. This systematically reduces $f_{b\bar{b}}$ from 0.229 to 0.215 in a roughly linear fashion, giving a sensitivity to $\Gamma_{c\bar{c}}$ of:

$$\Delta\Gamma_{b\bar{b}}/\Gamma_{b\bar{b}} = -0.135 \times \Delta\Gamma_{c\bar{c}}/\Gamma_{c\bar{c}}$$

This measurement technique is sensitive to charm only through the ratio:

$$\frac{\Gamma_{c\bar{c}}}{\Gamma_{u\bar{u}} + \Gamma_{d\bar{d}} + \Gamma_{s\bar{s}} + \Gamma_{c\bar{c}}}.$$

Within the Standard Model this ratio is predicted to great precision. If these Standard Model relative couplings are maintained, no systematic error need be attributed to this source. If no Standard Model constraints are used whatsoever, then the most precise direct determination of the charm partial width is a measurement by OPAL of the production rate for high momentum D^* mesons [20] which has a fractional precision of 22%. If only this measurement were used to constrain the charm fraction, this would lead to an additional uncertainty of $\Delta f_{b\bar{b}}=\pm 0.007$.

8.10 Charged Multiplicity

To gauge the size of potential uncertainties associated with the Monte Carlo modelling of light quark fragmentation, the Monte Carlo events were weighted to vary the mean charged multiplicity of the udsc component. The distribution of the charged multiplicity was weighted to vary the mean multiplicity between 20 and 24. This resulted in a change of the width of $\Delta f_{\mathrm{b\bar{b}}}=\pm 0.004$. Since the mean charged multiplicity of the data, 21.40 ± 0.02 ± 0.43 [21], is known to half a unit, a systematic uncertainty of $\Delta f_{\mathrm{b\bar{b}}}=\pm 0.001$ was attributed to the modelling of light quark fragmentation.

8.11 Event Selection

As a consistency check, the effects of changing the following event, track, and forward multiplicity selection requirements were studied:

- the minimum allowed $|\cos\theta_T|$ was varied between 0.866 and 0.707;
- the minimum allowed thrust of the events used in the analysis was varied between 0.80 and 0.90;
- the maximum allowed impact parameter for forward tracks was varied between 2.0 and 3.5 mm; and
- the minimum allowed impact parameter separation for forward tracks was varied between 2.4 and 3.0σ.

Varying the restriction on $\cos\theta_T$ results in a maximum change of $\Delta f_{\mathrm{b\bar{b}}}=0.003$. Changing the minimum allowed separation between 2.4 and 3.0σ changes $f_{\mathrm{b\bar{b}}}$ by $\Delta f_{\mathrm{b\bar{b}}}=\pm 0.003$. Varying the maximum allowed impact parameter changes $f_{\mathrm{b\bar{b}}}$ by less than $\Delta f_{\mathrm{b\bar{b}}}=\pm 0.004$. All of these changes are comparable to the expected statistical variations. Varying the restriction on the thrust between 0.80 and 0.93 changes the size of the event sample by $\pm 20\%$ and varies $f_{\mathrm{b\bar{b}}}$ between 0.226 and 0.216. The width was determined separately for each of 4 approximately equally populated bins between 0.8 and 1.0. Averaging the results for these 4 bins gives a value for $f_{\mathrm{b\bar{b}}}$ of 0.218 ± 0.007. An uncertainty of $\Delta f_{\mathrm{b\bar{b}}}=\pm 0.004$ has been assigned to account for a possible systematic trend as the thrust requirement is varied.

8.12 Event Generators

The systematic uncertainty associated with the choice of JETSET as the Monte Carlo event generator was studied by comparing 980 000 JETSET and 830 000 HERWIG events [22] gen-

erated using an approximate simulation of the detector. The two generators predict different distributions for the backwards multiplicity of $b\bar{b}$ events, and this can influence the fit. With this exception, there was no evidence that the choice of event generator leads to any systematic bias in the measurement.

The data and JETSET were examined for any difference in the $b\bar{b}$ backwards distribution by comparing the mean backward multiplicity of those hemispheres opposite a hemisphere with high forward multiplicity. No significant discrepancy was found.

Varying the backward $b\bar{b}$ distribution within the statistical uncertainty of the data-JETSET comparison resulted in a change in the width of $\Delta f_{b\bar{b}}=\pm 0.004$. A systematic uncertainty of this size has been assigned to account for possible deficiencies in the modelling of the backwards multiplicity of $b\bar{b}$ events.

8.13 Combined Systematic Uncertainty

A summary of the statistical and systematic uncertainties is presented in Table 3. The combined systematic uncertainty of $\Delta f_{b\bar{b}}=\pm 0.008$ was obtained by adding the individual contributions from all sources in quadrature.

9 Additional Checks

The fit for $f_{b\bar{b}}$ relies on the knowledge of the shapes of the four distributions in Equation 9. Discrepancies between the data and the Monte Carlo are taken into account by two parameters which allow the fit to change the shape of the Monte Carlo distributions. The parameter x accounts for discrepancies in the forward multiplicity of b jets. The parameter t accounts for discrepancies in the detector response. The fit determines x by effectively selecting events likely to be a B using one hemisphere and comparing the shapes of the forward multiplicity distributions in the other. The fit determines t by comparing the shapes of the data and Monte Carlo backward multiplicity distributions.

Reconstruction errors due to the higher multiplicity of b jets, for example, might lead to larger discrepancies for b events than for udsc events. Reconstruction errors in the dense core of a jet might lead to larger discrepancies for forward tracks than for backward tracks. Such effects can not be accounted for using a single parameter to describe the detector response, and could bias the fit.

These issues can be addressed by relaxing the assumption that only one parameter is needed to account for discrepancies in the detector response. The shapes of each of the four Monte Carlo

distributions can be allowed to change independently by introducing two additional parameters, a and d:

$$\begin{aligned} P^{\rm for}_{\rm udsc}(n_1,n_2) &\rightarrow P^{\rm for}_{\rm udsc}(n_1,n_2|t+a); \\ P^{\rm for}_{\rm b\bar{b}}(n_1,n_2) &\rightarrow P^{\rm for}_{\rm b\bar{b}}(n_1,n_2|x+t); \\ P^{\rm back}_{\rm udsc}(n_1,n_2) &\rightarrow P^{\rm back}_{\rm udsc}(n_1,n_2|t); \text{ and} \\ P^{\rm back}_{\rm b\bar{b}}(n_1,n_2) &\rightarrow P^{\rm back}_{\rm b\bar{b}}(n_1,n_2|t+d). \end{aligned} \tag{11}$$

The parameters x and t are determined by the fit. The parameter a allows for differences in the detector response for forward and backward tracks and the parameter d allows for differences between detector response for tracks in udsc and b hemispheres. Any systematic effect that can change the shapes of these distributions can be classified by its effect on these four parameters.

The size of a can be estimated by selecting an enriched sample of udsc events using one hemisphere and comparing the data and Monte Carlo forward multiplicity distributions in the opposite hemisphere. The size of d can be estimated selecting an enriched sample of b events using one hemisphere and comparing the data and Monte Carlo backward multiplicity distribution in the other.

Such a comparison yields values for a and d of:

$$\begin{aligned} a &= 0.004 \pm 0.003; \\ d &= 0.011 \pm 0.010. \end{aligned}$$

Varying these parameters within their statistical uncertainty changes $f_{\rm b\bar{b}}$ by

$$\Delta f_{\rm b\bar{b}} = -0.003 \pm 0.008.$$

Within the limited statistical precision of the check, there is no evidence of bias in the fitted value of $f_{\rm b\bar{b}}$. The result of this study is not treated as an additional systematic error but rather as an independent check that the magnitude of the systematic error estimates above are, indeed, reasonable.

10 Conclusion

The fractional partial width of the Z^0 to b quarks has been measured using an impact parameter technique to separate $Z^0 \rightarrow b\bar{b}$ events from the other hadronic decay channels. The method has been developed using 130 000 hadronic events collected by OPAL in 1990. We find:

$$\Gamma_{\rm b\bar{b}}/\Gamma_{\rm had} = 0.222 \pm 0.007 \text{ (stat)} \pm 0.008 \text{ (sys)}.$$

With the silicon micro-vertex detector installed in 1991 and the larger data samples collected during 1991 and 1992 we expect to improve both the statistical and systematic uncertainties.

This measurement assumes the relative rates of the Z^0 to uds and c quarks are given by the Standard Model. Varying the charm fraction from the Standard Model value of $\Gamma_{c\bar{c}}/\Gamma_{had}$=0.171 changes the result by $\Delta\Gamma_{b\bar{b}}/\Gamma_{b\bar{b}} = -0.135 \times \Delta\Gamma_{c\bar{c}}/\Gamma_{c\bar{c}}$. Allowing the charm fraction to vary by 22% (the precision of the best direct measurement) would lead to an additional systematic uncertainty of ± 0.007.

The result is in good agreement with the OPAL measurement [5] of $\Gamma_{b\bar{b}}$ using high momentum, high transverse momentum leptons to identify $Z^0 \to b\bar{b}$ events:

$$\Gamma_{b\bar{b}}/\Gamma_{had} = 0.220 \pm 0.002\ (\text{stat}) \pm 0.006\ (\text{sys}) \pm 0.011\ (\text{modelling}).$$

The modelling error includes systematic effects from b and c fragmentation and decay uncertainties and $\Gamma_{c\bar{c}}$.

The statistical and systematic errors of the two measurements are almost completely uncorrelated. The combined result is

$$\Gamma_{b\bar{b}}/\Gamma_{had} = 0.221 \pm 0.008\ (\text{stat+sys})$$

Uncertainties associated with $\Gamma_{c\bar{c}}$ have been excluded from this average. Allowing the charm fraction to vary by 22% will lead to an additional systematic uncertainty of ± 0.005. Combining this value with the total hadronic width measured by OPAL [1] ,

$$\Gamma_{had} = 1738 \pm 12\,\text{MeV},$$

yields the partial width of the Z^0 to b quarks,

$$\Gamma_{b\bar{b}} = 384 \pm 14\ (\text{stat+sys}) \pm 3\ (\text{hadronic width})\,\text{MeV}.$$

This is in good agreement with the prediction of the Standard Model for this partial width[4], 376 MeV.

Acknowledgements

It is a pleasure to thank the SL Division for the efficient operation of the LEP accelerator, the precise information on the absolute energy, and their continuing close cooperation with our

[4]This prediction was calculated using the ZFITTER lineshape program [23] with a top quark mass of 150 GeV/$c^2$and α_s=0.12. As the mass of the top quark is varied between 50 and 230 GeV/c^2, the prediction varies between 378 and 374 MeV.

experimental group. In addition to the support staff at our own institutions we are pleased to acknowledge the
Department of Energy, USA,
National Science Foundation, USA,
Texas National Research Laboratory Commission, USA,
Science and Engineering Research Council, UK,
Natural Sciences and Engineering Research Council, Canada,
Fussefeld Foundation,
Israeli Ministry of Energy and Ministry of Science,
Minerva Gesellschaft,
Japanese Ministry of Education, Science and Culture (the Monbusho) and a grant under the Monbusho International Science Research Program,
German Israeli Bi-national Science Foundation (GIF),
Direction des Sciences de la Matière du Commissariat à l'Energie Atomique, France,
Bundesministerium für Forschung und Technologie, Germany,
National Research Council of Canada,
A.P. Sloan Foundation and Junta Nacional de Investigação Científica e Tecnológica, Portugal.

References

[1] OPAL Collaboration, P. Acton et al., CERN/PPE 93–003 (13 January 1993) .

[2] The LEP Collaborations, Phys. Lett. B 276 (1992) 247;
L3 Collaboration, O. Adriani et al., CERN/PPE 93–31 (22 February 1993);
ALEPH Collaboration, D. Buskulic et al., CERN/PPE 93–40 (10 March 1993).

[3] A.A. Akhundov, D. Yu. Bardin and T. Riemann, Nucl. Phys. B 276 (1986) 1;
W. Beenakker and W. Hollik, Z. Phys. C 40 (1988) 141;
J. Bernabéu, A. Pich, and A. Santamaria, Nucl. Phys. B 363 (1991) 326;
B.W. Lynn and R.G. Stuart, Phys. Lett. B 252 (1990) 676.

[4] F. Boudjema, A. Djouadi, C. Verzegnassi, Phys. Lett. B 238 (1990) 423;
E. Nardi and E. Roulet, Nucl. Phys. B 248 (1990) 139;
M. Boulware and D. Finnell, Phys. Rev. D 44 (1991) 2054;
A. Djouadi et al., Nucl. Phys. B 349 (1991) 48;
R. Chivukula, S. Selipsky and E. Simmons, Phys. Rev. Lett. 69 (1992) 575.

[5] OPAL Collaboration, P. Acton et al., CERN/PPE 93–46 (9 March 1993) .

[6] DELPHI Collaboration, P. Abreu et al., Z. Phys. C 56 (1992) 47;
L3 Collaboration, B. Adeva et al., Phys. Lett. B 261 (1991) 177;
ALEPH Collaboration, D. Decamp et al., Phys. Lett. B 244 (1990) 551 .

[7] DELPHI Collaboration, P. Abreu et al., Phys. Lett. B 281 (1992) 383.

[8] DELPHI Collaboration, P. Abreu et al., Phys. Lett. B 295 (1992) 383;
L3 Collaboration, O. Adriani et al., CERN/PPE 93–60 (31 March 1993).

[9] Mark II Collaboration, R.G. Jacobsen et al., Phys. Rev. Lett. 67 (1991) 3347.

[10] OPAL Collaboration, K. Ahmet et al., Nucl. Instr. and Meth. A 305 (1991) 275.

[11] T. Sjöstrand, Comp. Phys. Comm. 39 (1986) 347;
T. Sjöstrand and M. Bengtsson, Comp. Phys. Comm. 43 (1987) 367.

[12] J. Allison et al., Nucl. Instr. and Meth. A 317 (1992) 47.

[13] OPAL Collaboration, M.Z. Akrawy et al., Z. Phys. C 47 (1990) 505.

[14] OPAL Collaboration, G. Alexander et al., Z. Phys. C 52 (1991) 175.

[15] OPAL Collaboration, P. Acton et al., Phys. Lett. B 274 (1992) 513.

[16] OPAL Collaboration, P. Acton et al., Phys. Lett. B 274 (1992) 513.

[17] M.S. Alam et al., Phys. Rev. Lett. 49 (1982) 357.

[18] C. Peterson et al., Phys. Rev. D 27 (1983) 105.

[19] Particle Data Group, K. Hikasa et al., Phys. Rep. 45 (1992) S1.

[20] OPAL Collaboration, G. Alexander et al., Phys. Lett. B 262 (1991) 341.

[21] OPAL Collaboration, P.D. Acton et al., Z. Phys. C 53 (1992) 539.

[22] G. Marchesini and B.R. Webber, Nucl. Phys. B 310 (1988) 461.

[23] D.Bardin et al., CERN–TH 6443/92, (May 1992).

n_2/n_1	0	1	2	3	4	5	6	7
0	**36391.0**	**26412.0**	**6563.0**	**1475.0**	**407.0**	**90.0**	15.0	3.0
	33434.4	**22042.8**	**3986.2**	**544.5**	**48.4**	**5.0**	0.5	0.0
	3150.6	**5003.6**	**2442.9**	**905.6**	**265.6**	**63.6**	11.7	2.5
1		**5606.0**	**3547.0**	**1151.0**	**327.0**	**65.0**	13.0	3.0
		3762.4	**1415.6**	**213.9**	**28.5**	**2.3**	0.5	0.0
		2029.5	**1993.7**	**736.3**	**222.3**	**44.7**	13.1	2.0
2			**759.0**	**552.0**	**171.0**	**48.0**	3.0	1.0
			144.3	**50.7**	**4.5**	**1.4**	0.0	0.0
			536.8	**413.2**	**122.6**	**29.8**	6.6	1.0
3				**115.0**	**74.0**	**18.0**	4.0	2.0
				5.0	**0.9**	**0.5**	0.5	0.0
				71.7	**52.2**	**7.6**	4.2	0.0
4					**12.0**	10.0	0.0	0.0
					0.0	0.0	0.0	0.0
					5.9	1.6	0.5	0.0
5						0.0	0.0	0.0
						0.0	0.0	0.0
						1.0	0.0	0.6

Table 1: The number of data and Monte Carlo events in each bin of forward multiplicity in the first hemisphere versus the forward multiplicity in the second. The first line for each bin shows the number of data events. The second shows the number of Monte Carlo events produced by udsc decays of the Z^0. The last line shows the number of Monte Carlo events produced by $b\overline{b}$ decays. The bins used in the fit are indicated by bold-faced type. The $b\overline{b}$ events have been weighted to reflect an average B hadron lifetime of $c\tau_B$=0.041 cm, and Monte Carlo has been normalized to the total number of data events to allow comparison. After the fit, the Monte Carlo distribution agrees well with the data at large n_1 and n_2.

n_2/n_1	0	1	2	3	4	5	6	7
0	**48329.0**	**26142.0**	**3827.0**	**442.0**	**35.0**	2.0	0.0	1.0
	37331.1	**21000.3**	**3008.4**	**313.4**	**26.7**	1.4	0.5	0.0
	10302.3	**5693.4**	**899.9**	**108.9**	**13.8**	0.0	0.0	0.0
1		**3643.0**	**1145.0**	**130.0**	**17.0**	1.0	1.0	0.0
		2945.1	**868.8**	**89.1**	**9.5**	0.9	0.5	0.0
		816.8	**232.7**	**37.7**	**5.3**	0.5	0.0	0.0
2			**93.0**	**22.0**	4.0	1.0	0.0	0.0
			71.5	**16.7**	4.5	0.9	0.5	0.0
			20.8	**8.8**	1.0	0.0	0.0	0.4
3				2.0	0.0	0.0	0.0	0.0
				2.3	0.0	0.5	0.0	0.0
				1.4	0.9	0.0	0.0	0.0
4					0.0	0.0	0.0	0.0
					0.0	0.0	0.0	0.0
					0.0	0.0	0.0	0.0
5						0.0	0.0	0.0
						0.0	0.0	0.0
						0.0	0.0	0.0

Table 2: The number of data and Monte Carlo events in each bin of backward multiplicity in the first hemisphere versus the backward multiplicity in the second. The first line for each bin shows the number of data events. The second shows the number of Monte Carlo events produced by udsc decays of the Z^0. The last line shows the number of Monte Carlo events produced by $b\overline{b}$ decays. The bins used in the fit are indicated by bold-faced type. The $b\overline{b}$ events have been weighted to reflect an average B hadron lifetime of $c\tau_B$=0.041 cm, and Monte Carlo has been normalized to the total number of data events to allow comparison.

Source	Contribution
Resolution	± 0.001
Non-Gaussian tails	± 0.001
B Lifetime	± 0.001
B Decay Multiplicity	± 0.004
b Fragmentation	± 0.001
Charm Modelling	± 0.002
c Fragmentation	± 0.001
Charged Multiplicity	± 0.001
Event Selection	± 0.004
Event Generator	± 0.004
Overall Systematic Error	± 0.008
Statistical Error	± 0.007

Table 3: A summary of the statistical and systematic uncertainties in the measured fractional width. The individual systematic errors were combined in quadrature to obtain the overall systematic error.

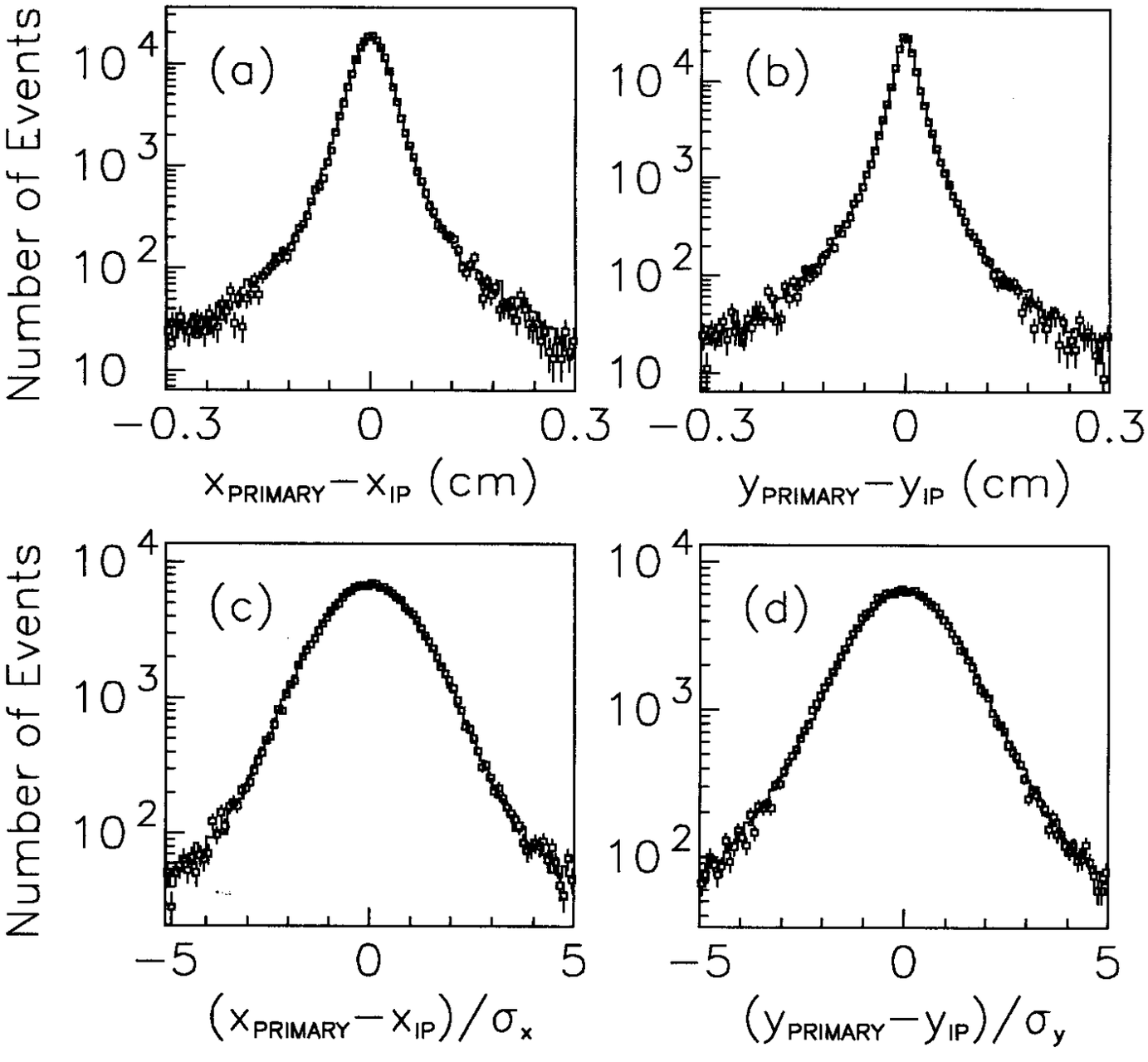

Figure 1: The distributions in x (a) and y (b) of the position of the unconstrained primary vertex with respect to the fill-by-fill beam centroid. The dimensionless separation in x and y of the primary from the beam centroid is plotted in (c) and (d). The data is represented by the squares in each of the plots while the distribution of the Monte Carlo primary is indicated by the solid line. The data is described well by the Monte Carlo.

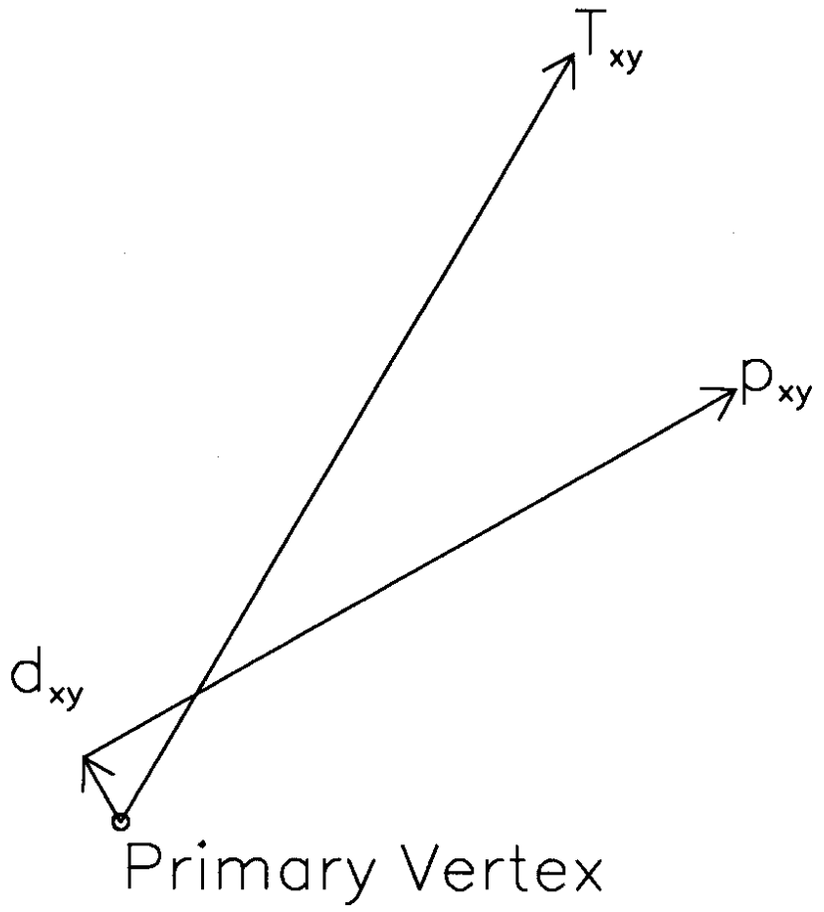

Figure 2: Schematic diagram showing the definition of the signed impact parameter.

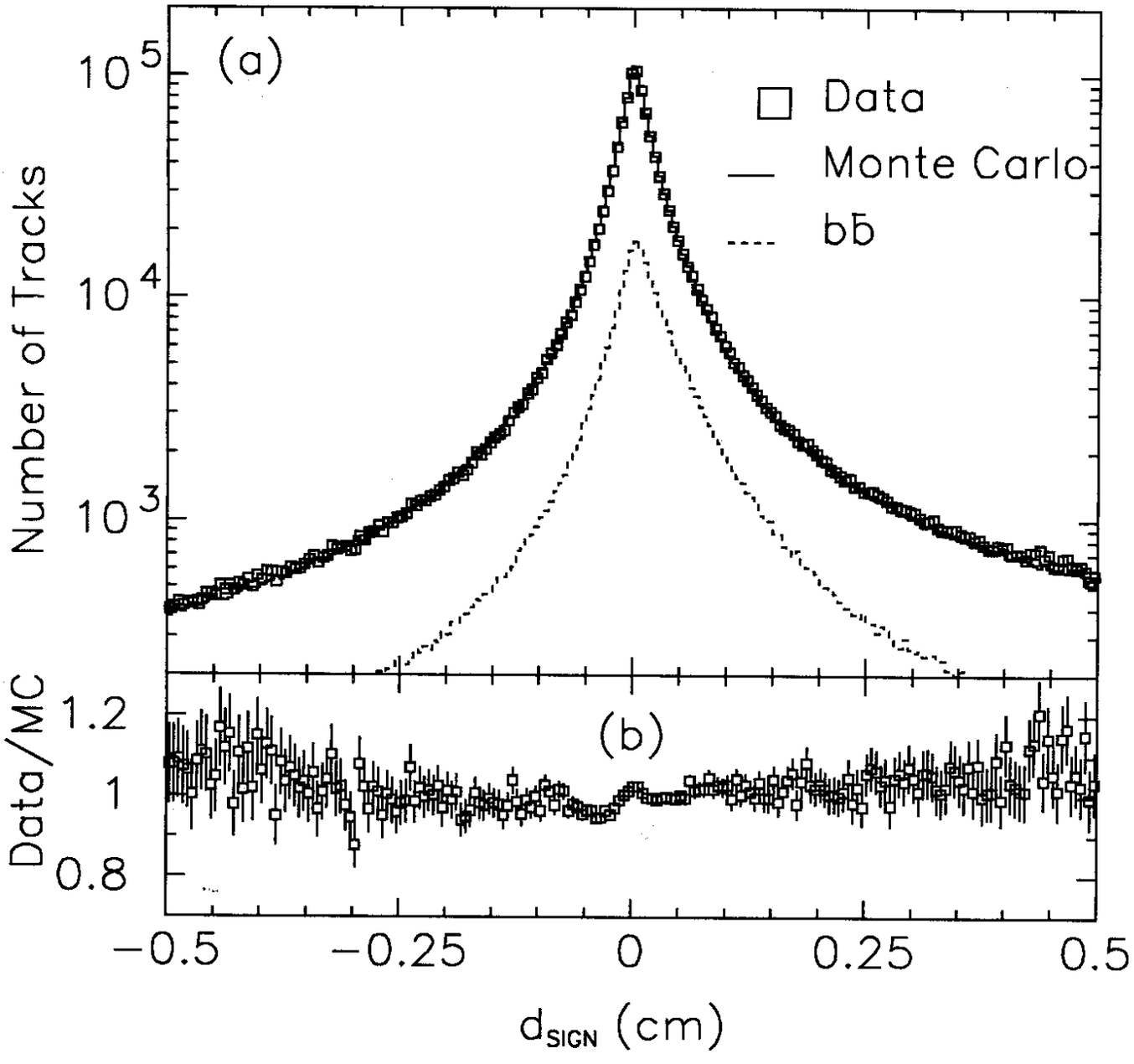

Figure 3: The distribution of the signed impact parameter for all the data tracks (squares) that meet the selection criteria. The solid line shows the same distribution for the Monte Carlo. The dashed line shows the $Z^0 \to b\bar{b}$ component of the Monte Carlo distribution. The ratio of the data to the Monte Carlo is shown in (b).

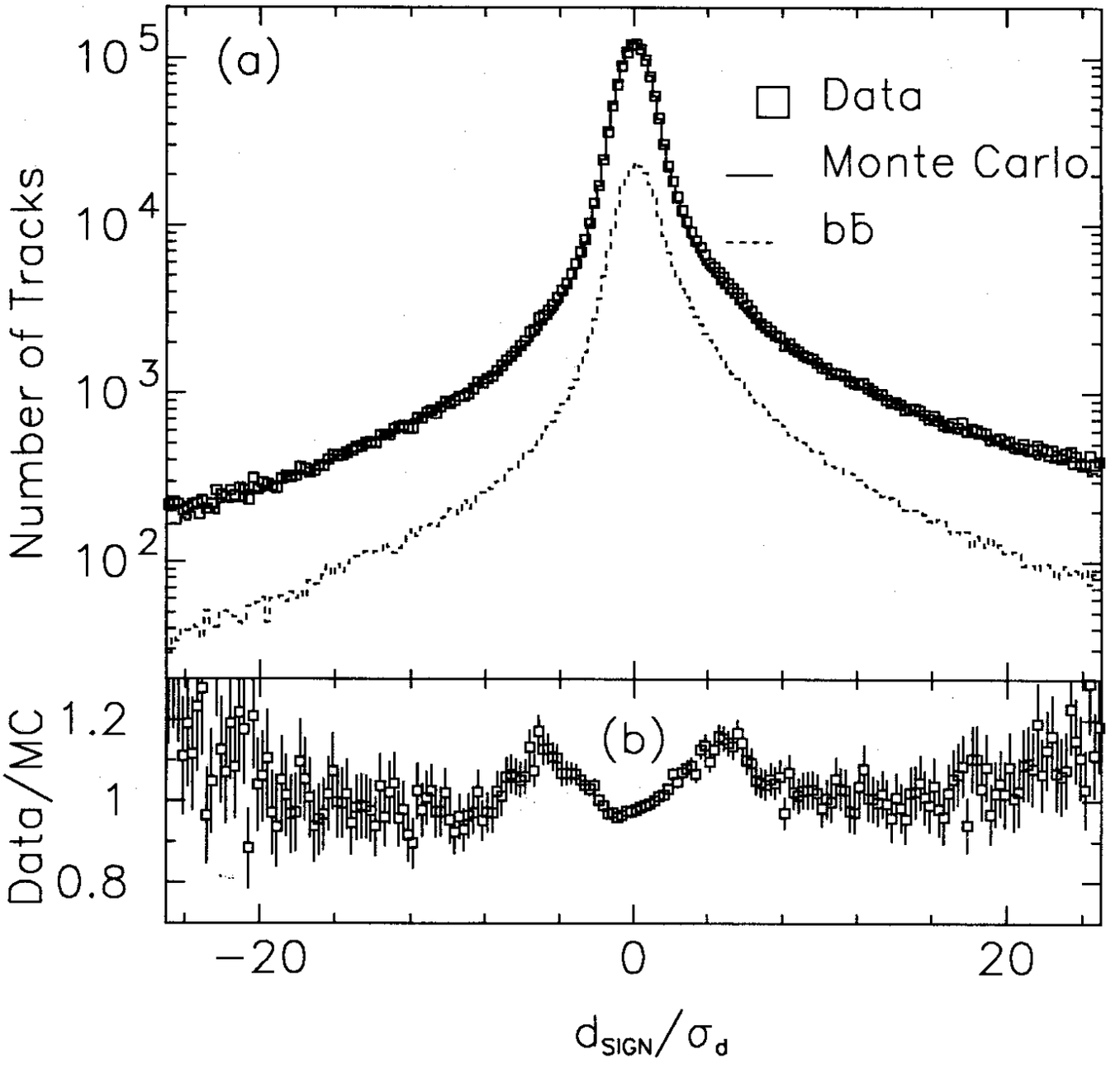

Figure 4: The separation for all selected tracks in the data (squares). The solid line shows the same distribution for the Monte Carlo. The dashed line shows the $Z^0 \to b\bar{b}$ component of the Monte Carlo distribution. The ratio of the data to the Monte Carlo is shown in (b).

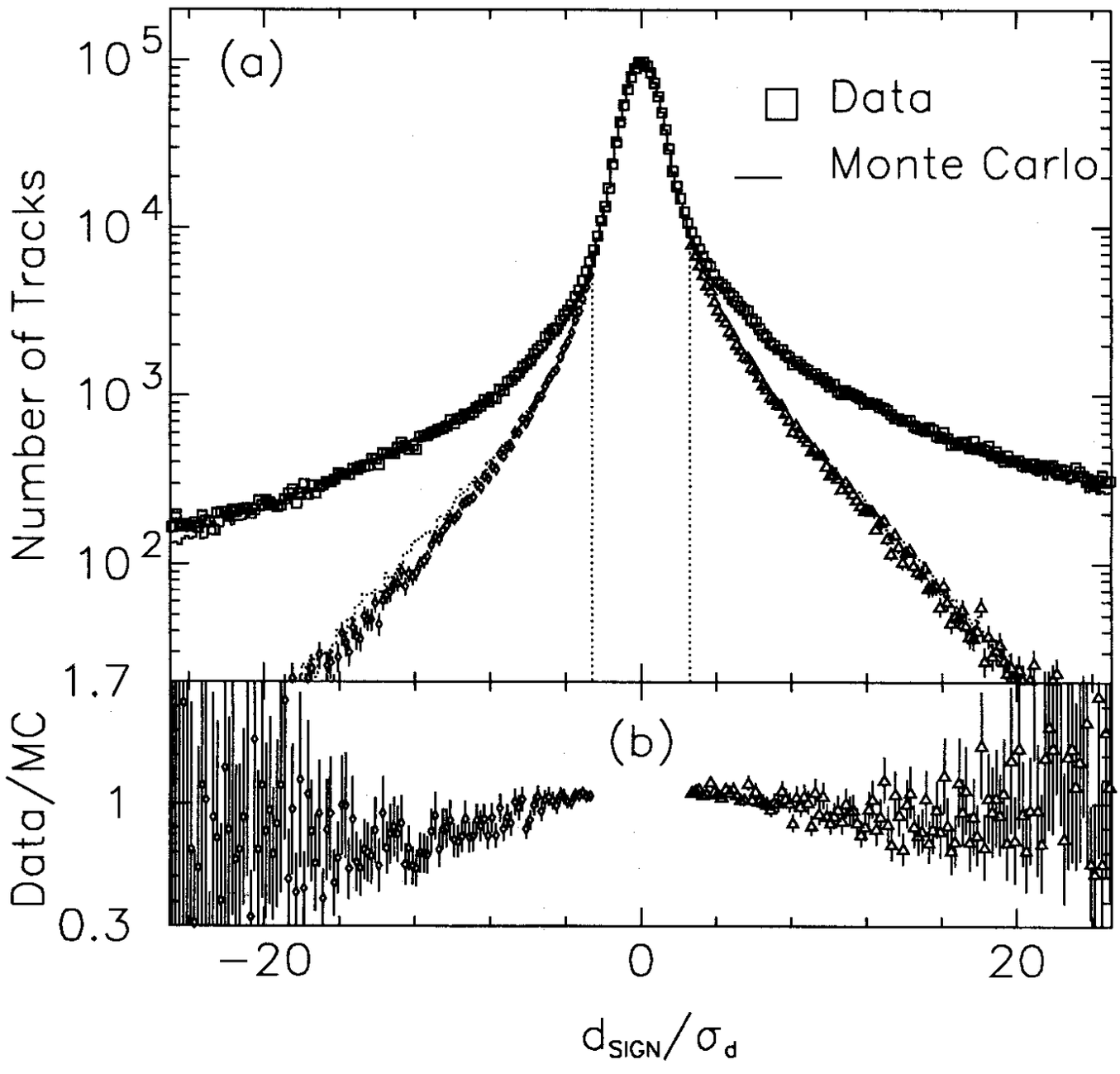

Figure 5: The distribution of signed separation, d_{sign}/σ_d, for all selected tracks in the data (squares). The triangles and diamonds show the same distribution for forward and backward tracks. The lines show the corresponding distributions for the Monte Carlo. The ratio of the data to the Monte Carlo for forward and backward tracks is shown in (b).

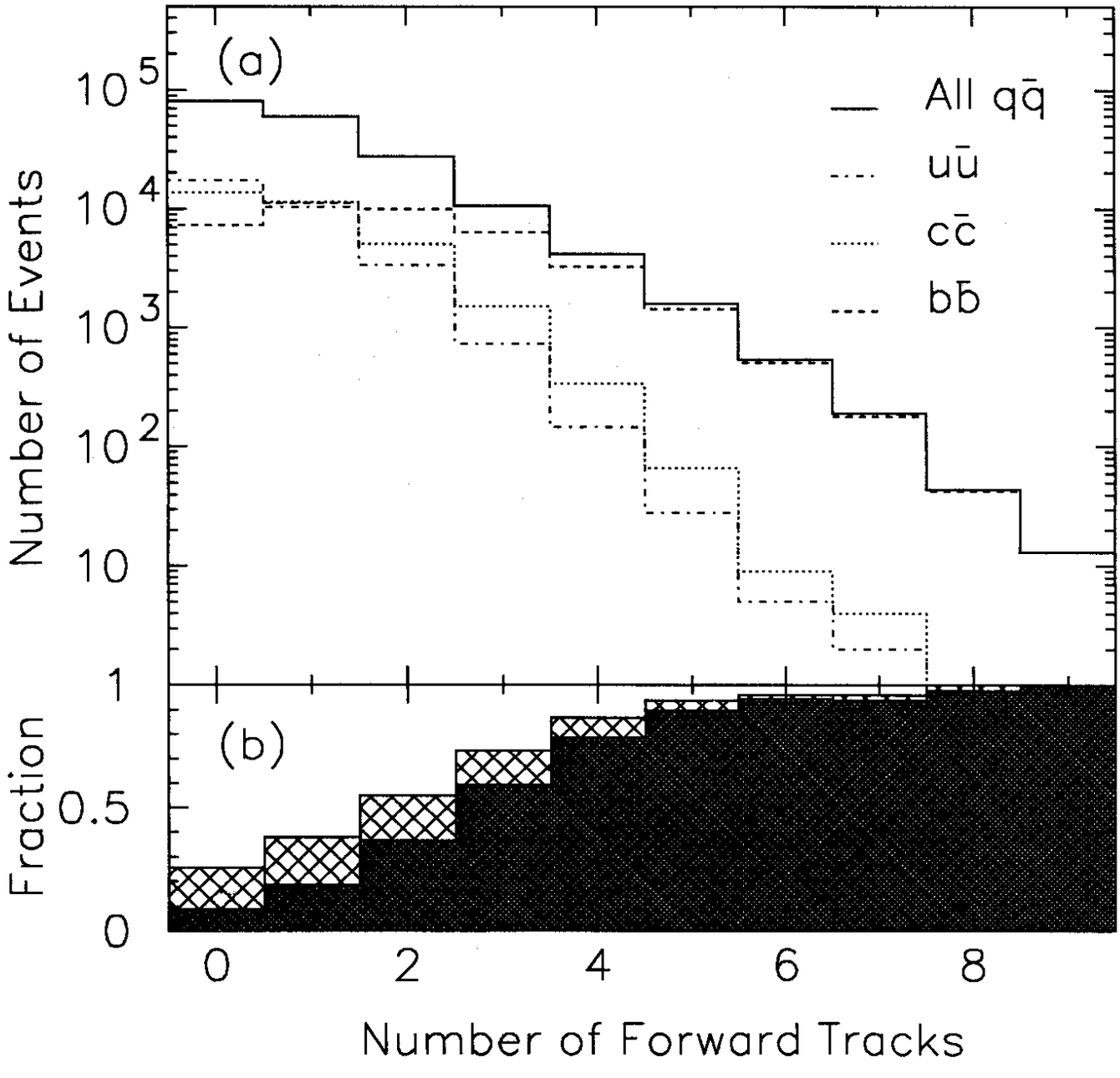

Figure 6: The forward multiplicity distribution for Monte Carlo events (solid line). The dashed line shows the $Z^0 \to b\bar{b}$ component predicted by the Monte Carlo. The dark region in (b) shows the fraction of events in each bin produced by $Z^0 \to b\bar{b}$ decays. The hatched region shows the fraction of events produced by $Z^0 \to c\bar{c}$.

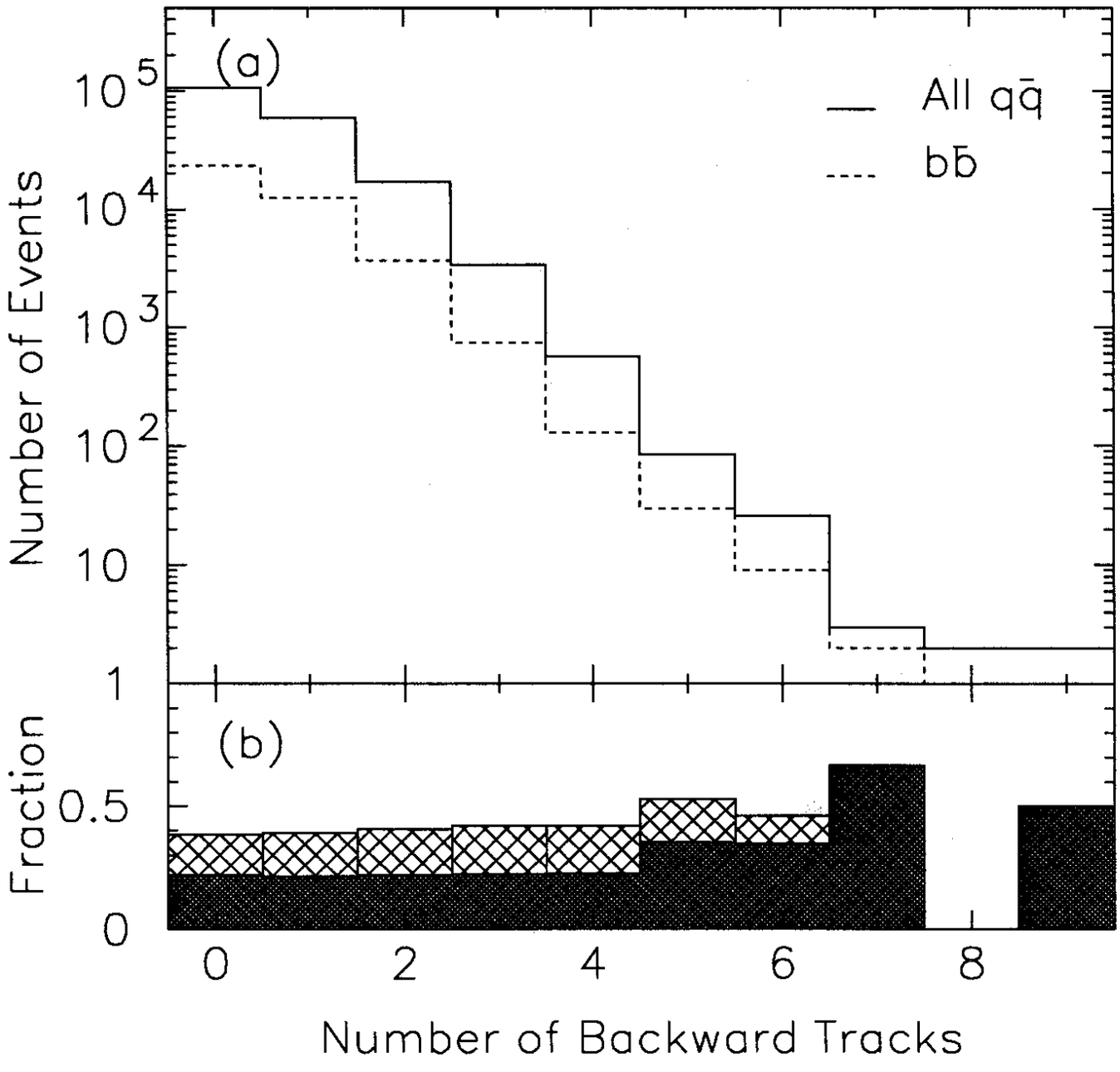

Figure 7: The backward multiplicity for Monte Carlo events (solid line). The dashed line shows the $Z^0 \to b\bar{b}$ component predicted by the Monte Carlo. The dark region in (b) shows the fraction of events in each bin produced by $Z^0 \to b\bar{b}$ decays. The hatched region shows the fraction of events produced by $Z^0 \to c\bar{c}$.

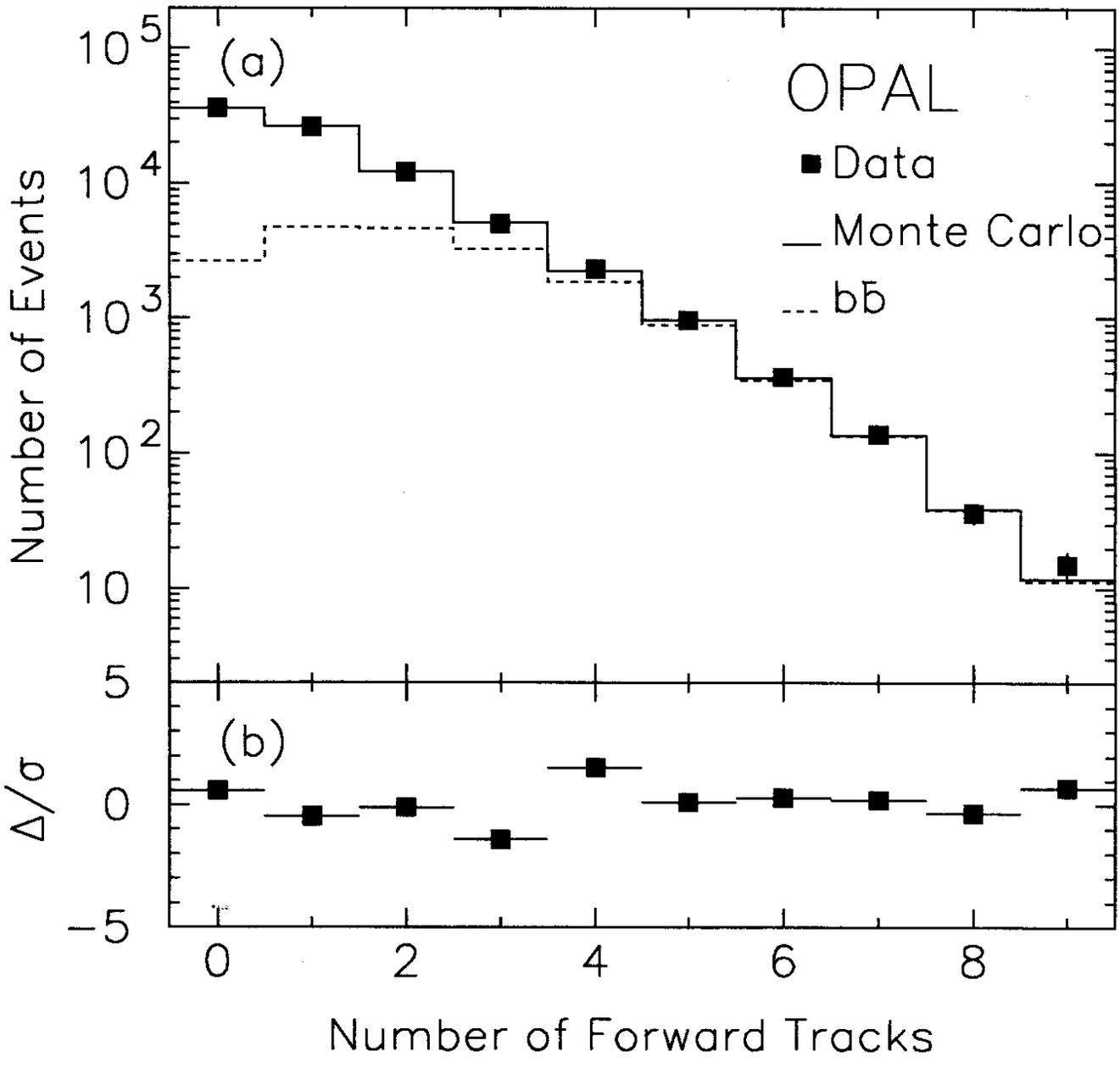

Figure 8: The distribution of forward multiplicity for the data events (squares). The solid line shows the distribution predicted by the Monte Carlo corrected using the results of the fit described in the text. The dashed line shows the $b\bar{b}$ component. The difference between the data and the Monte Carlo for each bin, Δ, divided by the statistical error for the bin, σ, is shown in (b).

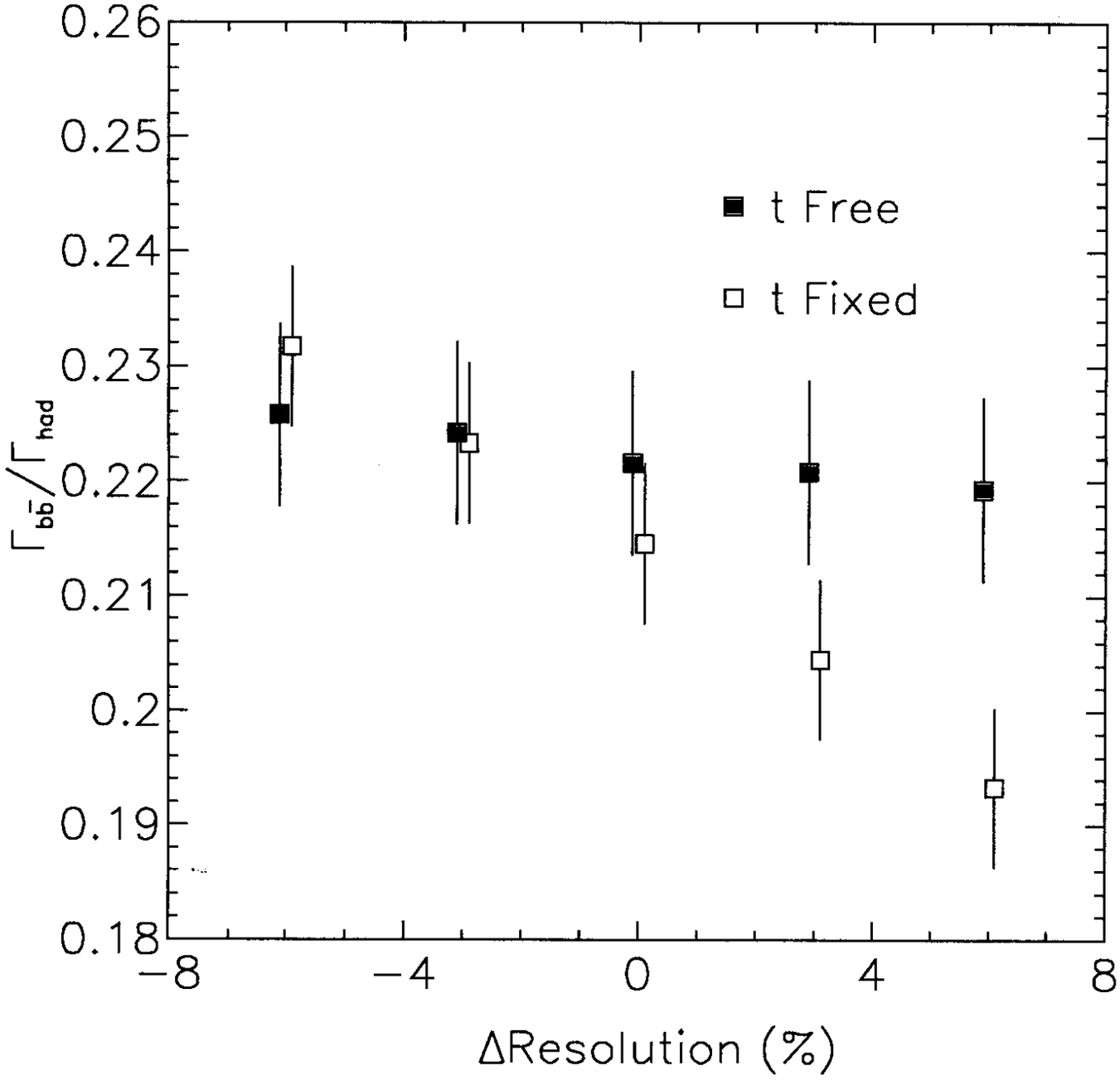

Figure 9: The fractional width determined by the fit with t as a free parameter (closed squares) when the Monte Carlo impact parameter resolution is varied. The open squares show the width determined when t is fixed to zero.

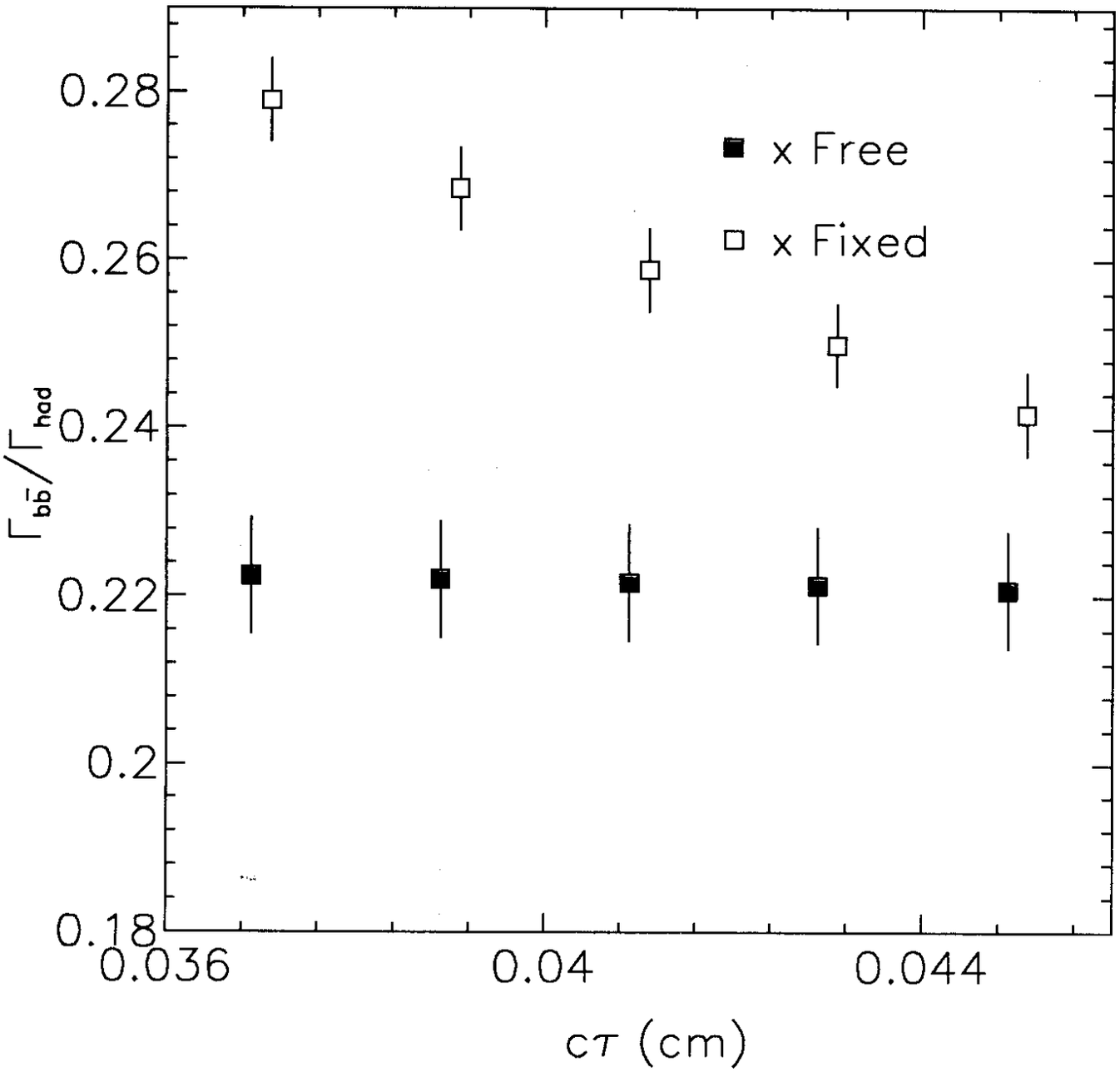

Figure 10: The fractional width determined by the fit with x as a free parameter (closed squares) when the Monte Carlo average B hadron lifetime is varied. The open squares show the width determined when x is fixed to zero.